ChemPubSoc Europe

DOI: 10.1002/cplu.201600235

CHEMPLUSCHEM Full Papers

Anode Preparation Strategies for the Electrocatalytic Oxidation of Water Based on Strong Interactions between Multiwalled Carbon Nanotubes and Cationic Acetylammonium Pyrene Moieties in Aqueous Solutions

Jacobus M. Koelewijn,[a] Martin Lutz,[b] Remko J. Detz,[a] and Joost N. H. Reek*[a]

A strategy is reported for the immobilization of iridium-based water oxidation catalyst **3** onto fluorine-doped tin oxide (FTO) anodes evaluated for the electrocatalytic oxidation of H_2O. The strategy is based on noncovalent π–π interactions between multiwalled carbon nanotubes (MWCNTs) and the cationic acetylammonium pyrene moiety (Pyr^+) covalently attached to a NHC $IrCp^*Cl_2$ catalytically active center (NHC = N-heterocyclic carbene, $Cp^* = C_5Me_5$). The dispersive properties of the Pyr^+ moiety in compound **3** leads to the formation of stable MWCNT dispersions in aqueous solutions. In addition, the MWCNT/**3** assembly shows activity in the Ce^{4+}-driven oxidation of H_2O. FTO/MWCNT/**3** anodes show increased current densities when used as a working electrode for the electrocatalytic oxidation of H_2O. At higher anodic polarizations initially high current densities were achieved; however, these currents prove to be non-sustained due to delamination and degradation of the catalytically active surface. The immobilization strategy is limited to applications below 1.4 V vs normal hydrogen electrode (NHE) as oxidation of the pyrene backbone is evident at higher potentials.

Introduction

The electrolytic oxidation of H_2O ($O_2 + 4H^+ + 4e^- \rightleftharpoons 2H_2O$; $E^\circ = 1.23$ V vs normal hydrogen electrode (NHE) at pH 0) is a key reaction for the conversion of solar energy into chemical energy, generating oxygen and hydrogen. The uncatalyzed reaction requires a large overpotential due to slow reaction kinetics at the (photo)anode interface. Next to the development of novel (molecular) electrocatalysts that drive the oxidation of H_2O, strategies are required that involve the surface immobilization of water oxidation catalysts (WOCs) onto anodes used for the electrolytic splitting of water. Molecularly anchored catalysts are mostly explored for ruthenium-based systems.[1–12] Other reports describe the electrocatalytic activity of molecular complexes based on nickel,[13] iron,[14] copper,[15–24] and cobalt[25–29] as well as their corresponding metal oxide films.[30–41] For iridium, very few well-defined molecular systems exist.[42–45] High current densities at low overpotentials are readily obtained by electrodes modified with IrO_2 films.[46–49] However, surface-immobilized "homogeneous" molecular catalysts have, in comparison to heterogeneous metal oxide films, the advantage that they can be fine-tuned by synthetic modification, for example in terms of the redox properties of the catalytically active site. In addition, active intermediates and mechanistic pathways can be studied in a more facile way. In economic terms, the use of a thin monolayer of a highly active molecular catalyst can have the advantage of a reduction in lower material costs. This paper describes an immobilization strategy based on noncovalent π–π interactions between the pyrene-functionalized NHC $IrCp^*Cl_2$ water oxidation catalyst **3** (NHC = N-heterocyclic carbene, $Cp^* = C_5Me_5$; Figure 1) and the graphene surface of multiwalled carbon nanotubes (MWCNTs). The strategy makes use of the properties of the cationic acetylammonium pyrene compound **1** (Pyr^+), which has been reported to facilitate the formation of stable dispersions/solutions of carbon nanomaterials in aqueous systems.[50–52] In aqueous systems the pyrene moiety acts as a hydrophobic anchor that binds to the graphene-type surface through π–π interactions and the ammonium moiety acts as a hydrophilic solubilizer. Reports on the application of compound **1** and related structures have been limited.[52–59] The compound has been used as a strong fluorescent marker but often the cationic nature of the acetylammonium pyrene scaffold **1** has been used for the electrostatic anchoring of polyanionic moieties such as DNA, quantum dots, tetrathiafulvalene, and (metallo)-porphyrins to graphene, single-walled carbon nanotubes (SWCNTs), MWCNTs, or even carbon nanohorns (CNHs).[60–66]

[a] *Dr. J. M. Koelewijn, Dr. R. J. Detz, Prof. Dr. J. N. H. Reek*
Van 't Hoff Institute for Molecular Sciences
University of Amsterdam
Science Park 904, 1098 XH Amsterdam (The Netherlands)
E-mail: j.n.h.reek@uva.nl

[b] *Dr. M. Lutz*
Crystal and Structural Chemistry Bijvoet Center for Biomolecular Research
Utrecht University
Padualaan 8, 3584 CH Utrecht (The Netherlands)

Supporting information (including a clear description of the experimental work) and the ORCID identification number(s) for the author(s) of this article can be found under http://dx.doi.org/10.1002/cplu.201600235.

This article is part of a Special Issue on "Catalytic Systems for Water Splitting". To view the complete issue, visit: http://dx.doi.org/10.1002/cplu.v81.10.

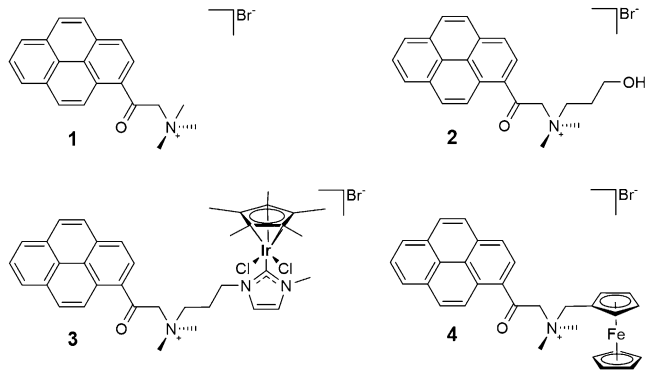

Figure 1. Structures of bare pyrene scaffolds **1** and **2**, and functionalized pyrene scaffolds **3** and **4**, carrying a NHC $IrCp^*Cl_2$ water oxidation catalyst and a ferrocene probe, respectively.

The group of Prato reported that photoexcitation of a Zn–porphyrin-based molecular sensitizer electrostatically bound to SWCNT/Pyr^+ or MWCNT/Pyr^+ assemblies results in long-lived radical ion pairs. Within this configuration, the carbon nanotube acts as the electron acceptor and the assembly as a whole forms a donor–acceptor nanohybrid, with Pyr^+ **1** as an essential part in the formation of the charge-separated state.[62,63,67,68] The assembly was used in a strategy for the preparation of photoanodes based on molecular compounds for the conversion of solar energy to electrical energy.[69–71] The Prato group also reported a similar strategy for the electrostatic immobilization of a ruthenium-based polyoxometalate on the surface of MWCNTs.[72,73] With respect to the use of MWCNTs as a support, Sun reported the immobilization and use of a pyrene-functionalized $Ru^{II}(L)(pic)_2$ water oxidation catalyst (pic = 4-picoline) onto indium tin oxide (ITO) electrodes coated by acid-treated MWCNTs.[74,75] Strategies involving carbon nanotubes for the fabrication of anodes have also been reported for inorganic electrocatalysts using the oxides of manganese, cobalt, and nickel[73,76–81] and in some cases CNTs are active electrocatalysts themselves.[82,83] Also electrochemical reduction of protons or CO_2 using a pyrene-functionalized catalyst anchored onto CNTs has been reported.[89–91] There are, however, no examples of molecular-based iridium water oxidation catalysts that, combined with MWCNTs, provide stable and efficient anodes that are active in the electrocatalytic oxidation of H_2O. In this report the properties of compound **1** as a dispersing agent for MWCNTs in aqueous solutions combined with the excellent catalytic properties of NHC $IrCp^*Cl_2$ are discussed.[84–87] This is realized by the direct covalent attachment of the catalyst to the pyrene anchor to obtain the novel catalytic precursor **3**. The propyl alcohol modified pyrene anchor **2** serves as a control for studying the adsorptive and electrocatalytic properties of MWCNT/Pyr^+ assemblies formed in aqueous solutions. In addition, compound **4** was designed as an electrochemical probe to study the stability of the MWCNT/Pyr^+ assemblies in operando, when immobilized onto fluorine-doped tin oxide (FTO)- and DropSens (DS)-based anodes, with respect to the electrocatalytic oxidation of H_2O.

Results and Discussion

Compound **1** (Pyr^+ Br^-) was readily prepared following a published procedure by introducing an excess of trimethylamine gas through a solution of 1-(bromoacetyl)pyrene in dry THF.[52] The yellow precipitate formed was isolated in quantitative yield by filtration. Compound **2** (Pyr^+–OH Br^-) was prepared by adding 2 equivalents of commercially available 3-dimethylamino-1-propanol to a solution of 1-(bromoacetyl)pyrene in dry THF after which the precipitate was filtered off. The solid was washed with Et_2O and dried under vacuum to provide a pure yellow amorphous compound in quantitative yield. For compound **3** (Pyr^+–Ir Br^-), the NHC backbone was first functionalized with an alkyl(dimethyl)amine linker before complexation with $IrCp^*Cl_2$ and attachment to the pyrene scaffold in the final step (Scheme 1). Starting from 3-dimethylamino-1-propanol, the respective chloride was obtained using thionylchloride in CH_2Cl_2 at 0 °C. Workup after 2 h yielded a white crystalline solid. Deprotection under basic conditions yielded the free amine, which was reacted with 25 equivalents of *N*-methylimidazole, solvent-free, at 80 °C for 24 h. The large excess was needed to prevent intermolecular reaction of the free amine. A viscous ionic liquid appeared after the reaction mixture had been washed repeatedly with Et_2O. Treating the ionic liquid with Ag_2O for 16 h in dichloromethane (DCM) yielded the silver carbene complex in situ which was further reacted with $\{IrCp^*Cl_2\}_2$. The dimethylamine-functionalized NHC $IrCp^*Cl_2$ turned out to be very hygroscopic, making it difficult to characterize. Instead, the isolated hygroscopic product was directly dissolved in anhydrous THF. Addition of 1-(bromoacetyl)pyrene to the solution yielded compound **3**; it precipitated from solution and therefore was filtered off as a yellow amorphous compound. Compound **4** was readily prepared by reacting commercially available {(dimethylamino)methyl}ferrocene with 1-bromoacetylpyrene under similar reaction conditions to provide compound **4** (Pyr^+–Fe Br^-) in a quantitative yield.

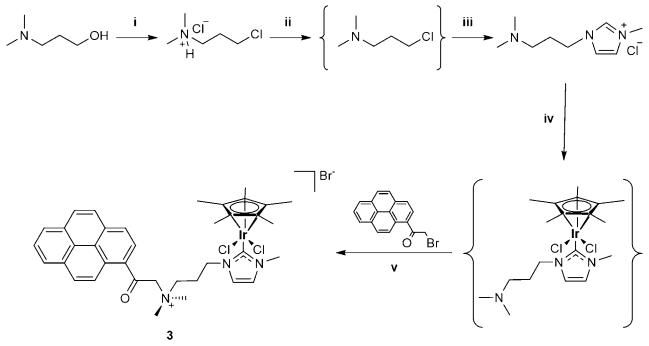

Scheme 1. Synthetic route towards pyrene-functionalized catalyst **3**: i) 1.0 equiv $SOCl_2$, DCM, 0 °C, 2 h; ii) K_2CO_3, H_2O, r.t., 1 h; iii) 25 equiv *N*-methylimidazole, 80 °C, 24 h; iv) Ag_2O, DCM, r.t., 24 h; v) (bromoacetyl)pyrene, THF.

The ^1H NMR spectrum of compound **3** dissolved in deuterated DMSO shows a complex splitting pattern in contrast to the spectra of compounds **1**, **2**, and **4**; this is attributed to steric

hindrance caused by the methyl groups on the Cp* moiety of the $IrCl_2$ complex (Figure S4). Compounds **1**–**4** were poorly soluble in a variety of organic solvents; however, anion exchange with PF_6^- (see the Supporting Information) greatly improved the solubility of **2** and **3** in acetone. Anion exchange is desirable as the presence of Br^- could interfere when one studies the electrocatalytic properties of **3** with respect to the oxidation of H_2O, as Br^- is easily oxidized (1.07 V vs NHE). In contrast to the bromide salts, the PF_6^- salts of compound **2** and **3** were insoluble in H_2O. Needle-like crystals of Pyr^+–OH PF_6^- **2** and Pyr^+–Ir PF_6^- **3** were grown by carefully layering pentane on top of a concentrated solution of the respective compound in acetone. The molecular structures of compound **2** and compound **3** were confirmed by X-ray crystal structure determination[92] (Figure S2 and Figure 2). The solid-state structure of compound **3** shows an iridium center with one coordinated DMSO solvent molecule and a coordinated halogen atom. Substitutional disorder indicates that the halogen is a mixture of chlorine and bromine in an approximate ratio of 1:1 (Figure S3). Modification of the NHC backbone does not induce significant changes in the coordination geometry of the catalytic center.[88] Compound **2** and compound **3** were reacted with cerium ammonium nitrate (CAN) used as a chemical oxidant to detect the formation of oxygen according to Equation (1).

$$2H_2O + 4Ce(IV) \xrightarrow{[Ir]} O_2 + 4H^+ + 4Ce(III) \quad (1)$$

The reaction was performed in the chamber of a Clark-type electrode to selectively detect oxygen. A solution of 130 μM **3** in 0.1 M HNO_3 at pH 1 was reacted with 50 mM CAN and compared to the reaction of **2** under the same experimental conditions. After an induction period of 10 seconds, O_2 formation is detected for **3** and is absent for **2** (Figure 3). This shows that the iridium center in **3** remains active for the catalytic oxidation of H_2O.[85]

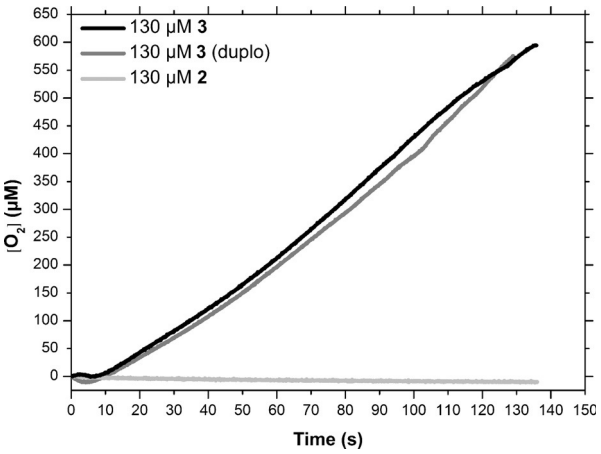

Figure 3. Proof of the catalytic activity of the iridium center in **3**. 130 μM solutions of **3** and **2** were reacted with 50 mM CAN in 0.1 M HNO_3., which generated oxygen [Eq. (1)]. Duplo means that the reaction was repeated under identical conditions, leading to two almost overlapping oxygen formation curves.

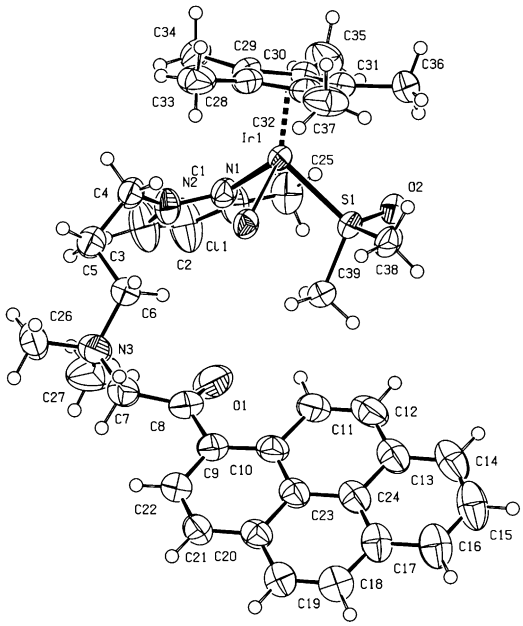

Figure 2. ORTEP representation of **3**[92] with ellipsoids at 50% probability level (PF_6^- counter ions and disordered solvent molecules not shown for clarity). Selected bond length and angle: Ir1-C1 2.066(6) Å, Cl1-Ir-C1 90.9(7)°.

Electrochemical measurements were performed for Pyr^+ Br^- compounds **2**–**4** dissolved in acetonitrile to study the potential window in which the organic framework is stable. It was found for all compounds that oxidation of the pyrene moiety occurs around 1.4 V vs NHE (Figure S5). To study compound **3** with respect to the electrocatalytic oxidation of H_2O in comparison to compound **2**, anodes were prepared by loading either compound **2** or **3** onto commercially available DropSens (DS) electrodes, which were used as the working electrode in a conventional three-electrode setup (see the Supporting Information). The DS working electrode consists of a screen-printed, carbon electroactive surface modified with MWCNTs. In this way the interaction of the Pyr^+ anchor with the MWCNT surface could be explored (Figure S1).

Figure 4 shows the current–potential (I–V) curves of a typical experiment. First a DS electrode was used in a blank measurement using a 0.1 M phosphate buffer solution at pH 2.0. After rinsing with demineralized water and drying, the same DS anode was loaded by dropcasting 100 μL of an 0.2 mM solution of compound **2** or **3** in MeCN onto the electroactive surface area of the DS anode after which the DS anode was submerged in the 0.1 M phosphate buffer solution and the potential swept to 1.8 V vs NHE (Figure 4). For compound **2** (Figure 4a) after the first anodic scan, two irreversible oxidation waves are observed with an onset potential of 1.09 V and 1.37 V vs NHE, corresponding approximately to the oxidation potentials of the Br^- anion and the pyrene moiety measured with respect to ferrocene as shown in Figure S5. Both waves decrease in intensity upon sequential scanning of the DS/**2** anode and a second reversible redox wave appears at the

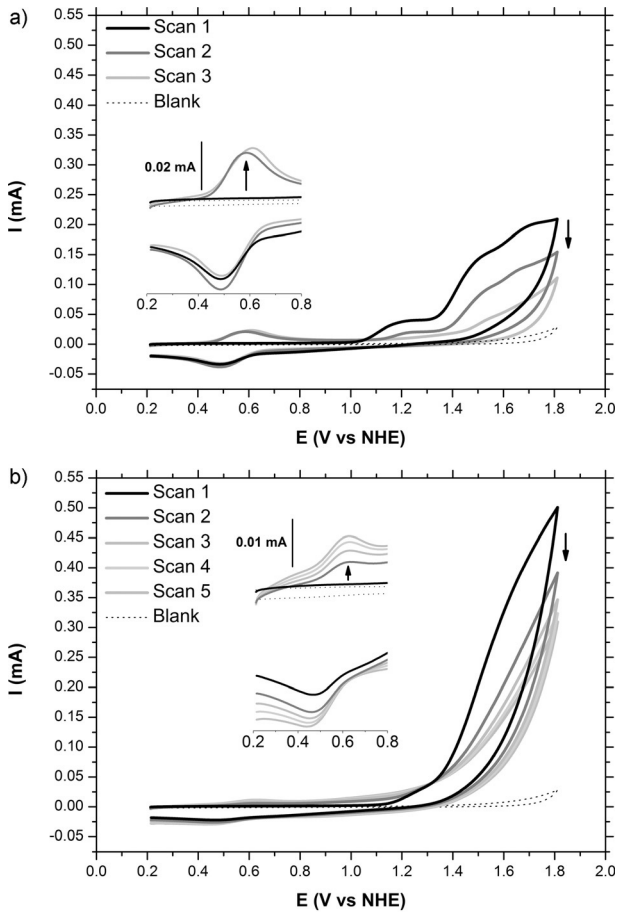

Figure 4. I–V curves for experiments comparing the electrocatalytic activities of **2** and **3**. a) 100 μL 0.2 mM **2** and b) 100 μL 0.2 mM **3** in MeCN dropcast onto a DS electrode. The electroactive surface area of the DS anode is 0.1 cm^2. A Pt coil was used as the counter electrode and a Ag/AgCl (3 M KCl) electrode was used as a reference electrode with (E° (V vs Ag/AgCl) = +0.21 V vs NHE).

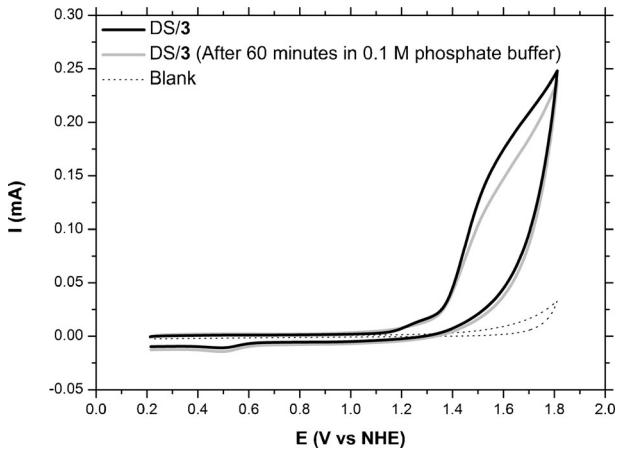

Figure 5. I–V curves for experiments showing the desorption of **3** from a DS anode. DS/**3** working electrode was prepared by dropcasting 30 μL 0.2 mM **3** in MeCN applied directly (black trace) and the second electrode was subsequently submerged for 60 min in an 0.1 M phosphate buffer solution (gray trace). A Pt coil was used as the counter electrode and a Ag/AgCl (3 M KCl) electrode was used as a reference electrode with (E° (V vs Ag/AgCl) = +0.21 V vs NHE).

second and third scan with a well-defined $E_{1/2}$ potential of 0.54 V vs NHE (Figure 4a, inset). For Pyr^+ Br^- **3** (Figure 4b) the I–V curve shows a feature evident for a catalytic wave with a current density of 4.9 mA cm^{-2} at 1.8 V vs NHE. After the initial anodic sweep a similar feature with an $E_{1/2}$ potential of 0.54 V vs NHE grows in intensity (Figure 4b, inset) while the total current density at 1.8 V vs NHE decreases. This feature found for **2**, **3**. and **4** is assumed to correspond to the degradation of the molecular framework adsorbed on the electrode surface after oxidation of the pyrene moiety has occurred (Figures S5–S9). The decrease in current density after successive scanning can be explained by the desorption of **3** from the DS anode during the experiment as the bromide salt of compound **3** is moderately soluble in H_2O. To confirm this, two DS anodes were dropcast with 30 μL 0.2 mM **3** and one of these was submerged in a 0.1 M phosphate buffer solution for 60 min prior to the first anodic sweep. Figure 5 shows that no desorption has occurred within 60 min, as no significant decrease in current density is observed at the initial scan compared to the DS/**3** anode that was not submerged in the phosphate buffer solution (Figure 5). This indicates that the decrease in intensity as observed in Figure 4b is not due to direct desorption of the catalytic precursor. It is therefore most likely due to degradation of the Pyr^+ anchor at high anodic potentials followed by desorption of degradation products of compound **3**. However, catalyst deactivation or leaching of the oxidized pyrene or activated (higher oxidized) iridium species cannot be ruled out at this point. The absence of desorption of catalytic precursor **3** from the DS anode indicates that the molecular precursor remains adsorbed to the DS/MWCNT surface. In addition, experiments performed with electrochemical probe **4** showed that spontaneous adsorption of the Pyr^+ moiety to the MWCNT surface occurs when a blank DS anode was submerged overnight in an 0.2 mM aqueous solution of **4** (Figure S8). Both experiments confirm the strong interaction of the Pyr^+ moiety with the DS/MWCNT surface in an aqueous environment.

The propensity of the cationic pyrene anchor to disperse MWCNTs in aqueous solutions, reported for Pyr^+ Br^- **1**,[52] was also observed for Pyr^+ Br^- **2**, Pyr^+ Br^- **3**, and Pyr^+ Br^- **4**. For Pyr^+ Br^- **3**, this observation was used to devise a strategy for constructing FTO anodes for the electrolytic splitting of H_2O. In a typical experiment a vial filled with 5 mL of 0.2 mM **3** was left to stir overnight in the presence of 5 mg MWCNTs. After ultrasonification of the mixture a stable black dispersion of the MWCNTs in water is obtained as shown in the left vial in Figure 8a. The catalytic iridium center of **3** is now immobilized on the MWCNT surface while the cationic Pyr^+ anchor of compound **3** prevents the MWCNTs to conglomerate. The adsorption conditions were selected to assure full adsorption of Pyr^+ Br^- **3** to the MWCNTs so to minimize traces of leftover compound **3** in the supernatant solution (Figures S10–S12).

The MWCNT/**3** assembly was isolated after centrifugation of the mixture and decantation of the supernatant solution. The successful immobilization of **3** on the MWCNT surface is demonstrated when it is reacted with CAN in the reaction chamber

of a Clark-type electrode, in analogy to the experiments presented in Figure 3. Rapid visible evolution of O_2 was observed in contrast to experiments with pristine MWCNTs exposed to the same CAN concentration (Figure 6). When the isolated

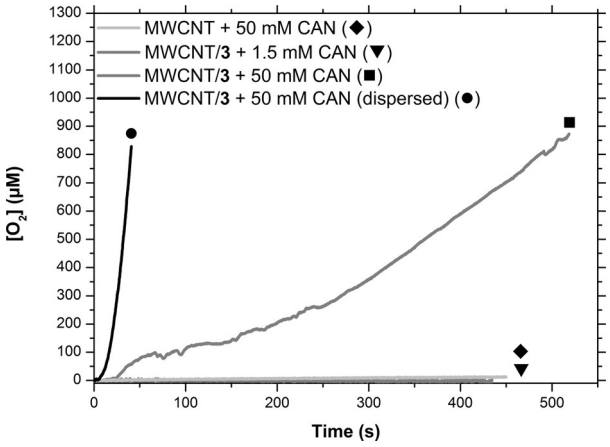

Figure 6. O_2 evolution curves measured using a Clark-type electrode of MWCNT/**3** in 0.1 M HNO_3 at pH 1.0.

MWCNT/**3** assemblies are dispersed by ultrasonification, the activity is higher than that observed for nondispersed MWCNT/**3** assemblies, which were simply isolated by decantation of the supernatant prior to the ultrasonication step. Dispersion of the assembly probably ensures full exposure of catalytically active sites. When lower concentrations of CAN were employed (▼ in Figure 6), no O_2 formation was observed.

The experiments demonstrate that assemblies of **3** and MWCNTs can be formed in aqueous solutions which, when isolated, remain catalytically active for the Ce^{4+}-driven oxidation of H_2O (Figure 7). The maximum loading reached corresponds to a total loading of approximately 0.25 mmol Pyr^+/g MWCNT, which is unaffected by changes in pH or ionic strength in the case of aqueous solutions yet strongly shifts in MeOH solutions (Figures S10 and S11).

FTO anodes were prepared by dropcasting 100 μL of black aqueous dispersions of MWCNTs prepared using either Pyr^+ Br^- **2** or Pyr^+ Br^- **3**, according to the previously described procedure, thereby completely covering the FTO surface without loss of the dropcast volume. After dropcasting, the FTO anodes were left to dry in air for a few hours (Figure 8b). To compare the effect of additional layering, after the drying step,

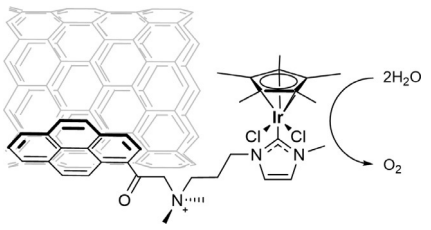

Figure 7. Proposed immobilization of **3** on the MWCNT surface and O_2 generation (see Figure 6).

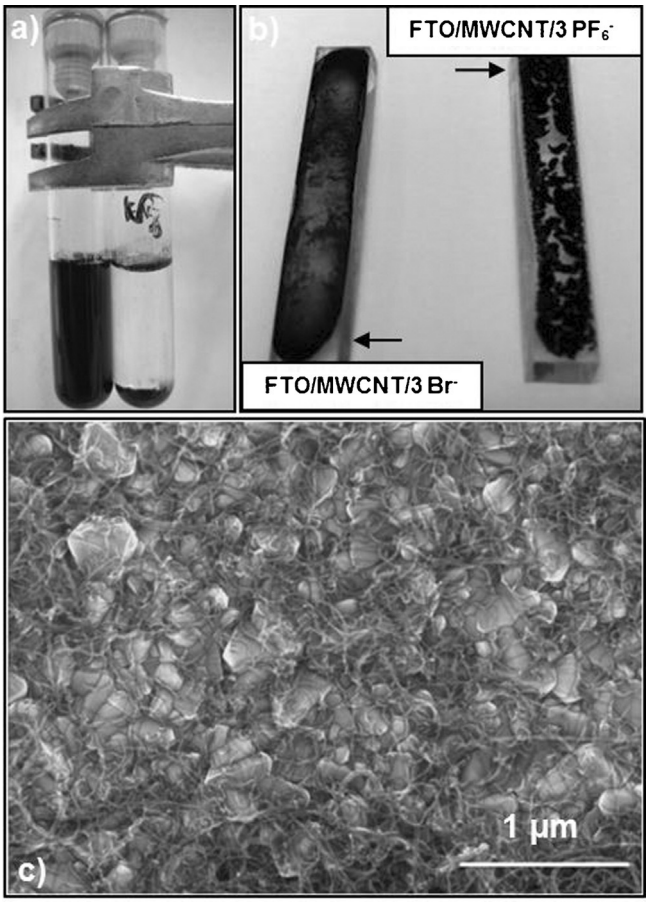

Figure 8. a) Black stable suspension obtained for MWCNT/Pyr^+ Br^- **3** assembly in demineralized H_2O (left) and the absence of a stable suspension for MWCNT/Pyr^+ PF_6^-. (right). b) FTO substrates after dropcasting of 100 μL of the respective dispersions. Delamination is readily observed for MWCNT/**3** PF_6^-. c) SEM image of the FTO/MWCNT/**3** Br^- anode surface, 20.0 kV, 3.0 Spot 25 000×.

a subsequent layer was applied by dropcasting 100 μL of the supernatant, and this step was repeated to provide FTO anodes with various layer thicknesses (prepared by dropcasting 100–300 μL) of MWCNT/Pyr^+. In one experiment, the aqueous dispersions of MWCNT/**2** and MWCNT/**3** were treated (prior to dropcasting) by adding KPF_6 to the supernatant solution after a 3.5 h adsorption period in an attempt to exchange the electrochemically active Br^- anion for PF_6^-. Figure S12 depicts the effect of the anion exchange by showing that no traces of Pyr^+ in the supernatant are detected after addition of KPF_6. The low solubility of Pyr^+ PF_6^- in H_2O, as discussed previously, probably results in precipitation of the salt on the MWCNT surface. As a result the dispersive property of the cationic Pyr^+ anchor was lost and stable MWCNT dispersions could not be formed (right vial in Figure 8a). Dropcasting of the MWCNT/Pyr^+ assemblies, which were treated with KPF_6, resulted in poor-quality anodes of which the MWCNT layer readily cracks and delaminates (Figure 8b). This demonstrates the importance of the dispersing property of the Pyr^+ moiety in the anodes, as the MWCNT/Pyr^+ assemblies prepared without KPF_6 result in a uniform MWCNT/Pyr^+ film on the FTO surface.

FTO anodes prepared via this strategy with $Pyr^+ Br^-$ **4** display good electrochemical communication between the molecular probe present in the MWCNT/**4** assembly and the electrode, as a proper response of the ferrocene redox couple in **4** is observed upon successively sweeping the anode potential between 0.0 V and 0.6 V vs Ag for more than 50 times (Figure S9).

FTO/MWCNT/**2** and FTO/MWCNT/**3** anodes prepared with MWCNT/Pyr^+ layers of various thicknesses (prepared by dropcasting 100 to 300 μL of the dispersion) were used directly as the working electrode in a three-electrode configuration with a Ag/AgCl (3 M KCl) reference electrode and a Pt-coil counter electrode submerged in a 0.1 M phosphate buffer solution at pH 2.0. The cyclic voltammogram (CV) for FTO/MWCNT/**2** (Figure 9a) shows the onset for the oxidation of pyrene at ca. 1.4 V vs NHE. The signal intensity increases in accordance with the anticipated increase in the thickness of the MWCNT/**2** layer deposited on the FTO surface by using higher dropcasting volumes. This clearly indicates that the molecular identity of **2** attached to the MWCNT surface is retained. Repeated scanning (Figure 9b) resulted in a minor reduction in current density accompanied by the disappearance of the pyrene oxidation wave and the appearance of the redox wave with $E_{1/2} = 0.54$ V vs NHE. As previously discussed for the experiments using the DS anodes, this wave is ascribed to decomposition products formed once oxidation of the pyrene moiety has occurred (Figure S9). For FTO/MWCNT/**3** (Figure 9c) a similar trend is observed and the current density is significantly increased compared to that of FTO/MWCNT/**2** (from ca. 0.5 mA cm^{-2} to ca. 1.5 mA cm^{-2}) determined at 1.5 V vs NHE for the first scan of the anode prepared with the highest layer thickness (300 μL). This increased current density of FTO/MWCNT/**3** is attributed to the electrocatalytic oxidation of H_2O by **3**. In some of the experiments, delamination upon immersion of the modified FTO anodes in the electrolyte solution was observed, indicating that multiple layering of the FTO anode by simple dropcasting is not a suitable method for the preparation of robust functional anodes. Therefore from this point onward, anodes prepared by depositing one layer (100 μL) of the respective dispersions are used.

In general, scanning at higher potentials leads to decomposition at a molecular level (Figure S9). Therefore freshly prepared FTO/MWCNT/**3** anodes were scanned to a maximum of 1.6 V and 1.4 V vs NHE and the results are depicted in Figure 10a,b respectively. Scanning to 1.6 V shows that the initially high current density of 1.7 mA cm^{-2} rapidly decreases and the degradation products of **3** again become apparent at 0.54 V vs NHE. Scanning to 1.4 V the potential remains just below the oxidation potential of pyrene. A small decrease in the current density is still apparent, yet the buildup of decomposition products increases to a smaller extent as depicted in the inset of Figure 10b. Freshly prepared anodes of FTO/MWCNT/**2** and FTO/MWCNT/**3** were subjected to extended use

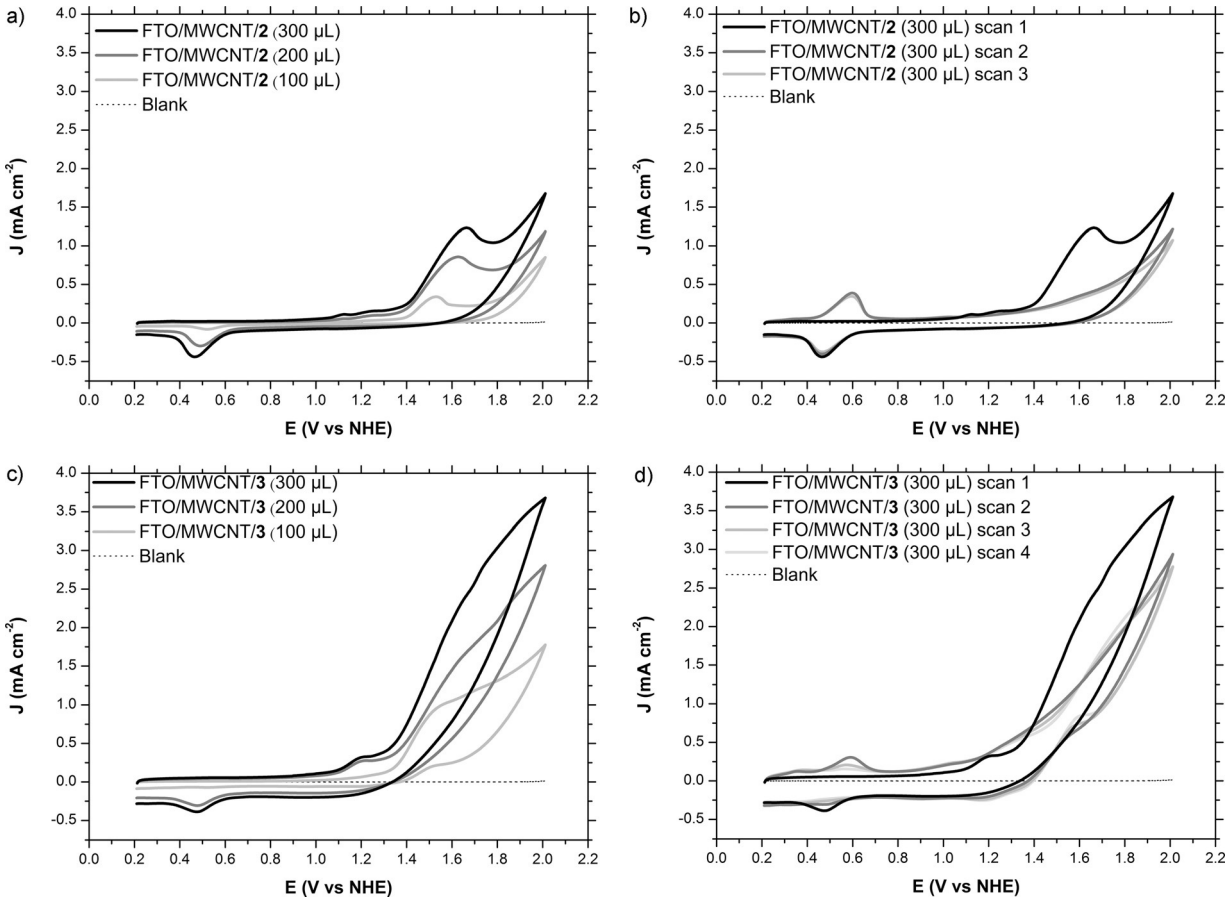

Figure 9. Cyclic voltammograms for FTO/MWCNT/**2** (a, b) and FTO/MWCNT/**3** (c, d) used as the working electrode in 0.1 M phosphate buffer solution at pH 2.0 and scanspeed 0.1 V s^{-1}. Anodes were prepared with various MWCNT/Pyr^+ layers of various thicknesses and subjected to successive scans.

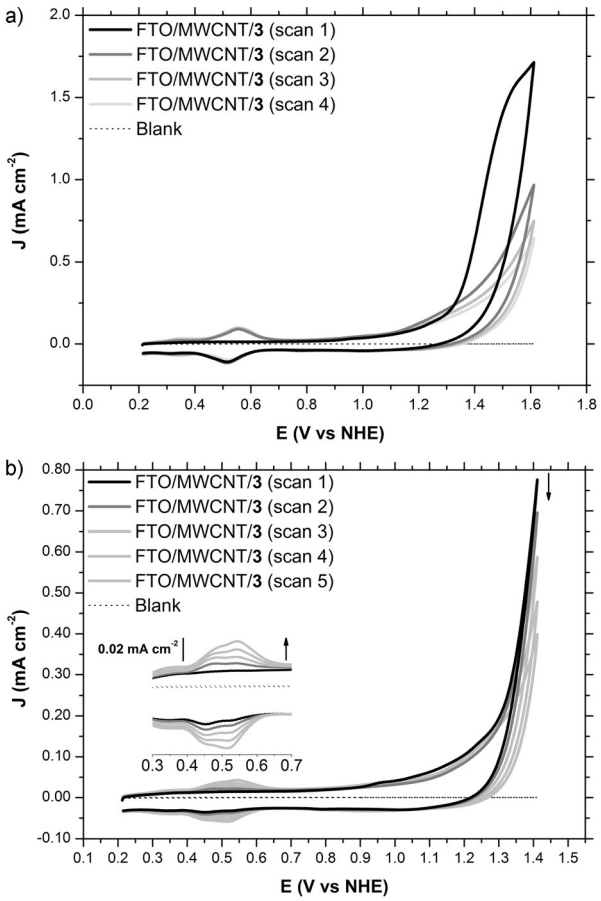

Figure 10. FTO/MWCNT/**3** used as the working electrode in 0.1 M phosphate buffer solution at pH 2.0 at scanspeed 0.1 V s^{-1}; a) scans up to 1.6 V, b) scans up to 1.4 V.

by applying subsequent on/off cycles at 1.8 V vs NHE to study the stability of the prepared anodes in terms of the observed current density (Figure 11). The difference in current density observed for the initial on/off cycles between FTO/MWCNT/**2** and FTO/MWCNT/**3** is attributed to water oxidation catalysis. This significant change in current density decreases with each successive cycle as the current density of FTO/MWCNT/**3** decreases while the current density in FTO/MWCNT/**2** remains consistent. This decrease in current density after repeated, successive scanning is in line with leaching of the catalytically active center after decomposition of the linker. Similar experiments at pH 6.8 show that the catalyst is not sufficiently active under these conditions, but suggest that the anchoring strategy can be used at this pH.

In a control experiment, the prolonged activity of FTO/MWCNT/**3** in a phosphate buffer solution at pH 2.0 was compared at 1.4 V and 1.8 V vs NHE (Figure 12). At 1.8 V vs NHE the formation of bubbles was clearly observed on the anode's surface in contrast to the experiment at 1.4 V vs NHE. Bubble formation halted after ca. 800 seconds, in accordance with the decrease in current density.

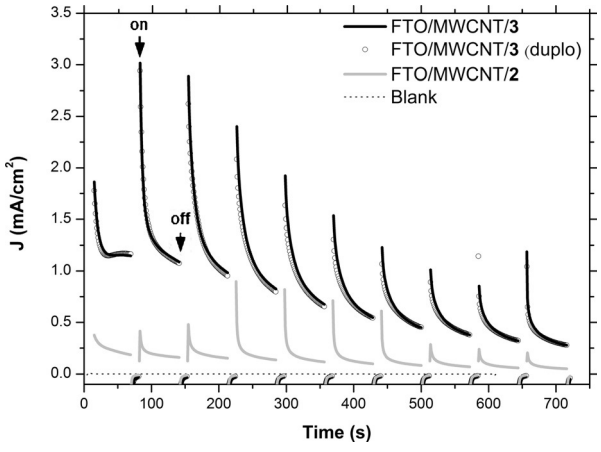

Figure 11. Stability of FTO/MWCNT/**2** and FTO/MWCNT/**3** anodes subjected to repeated on/off cycles at 1.8 V vs NHE [1] in 0.1 M phosphate buffer solution at pH 2.0.

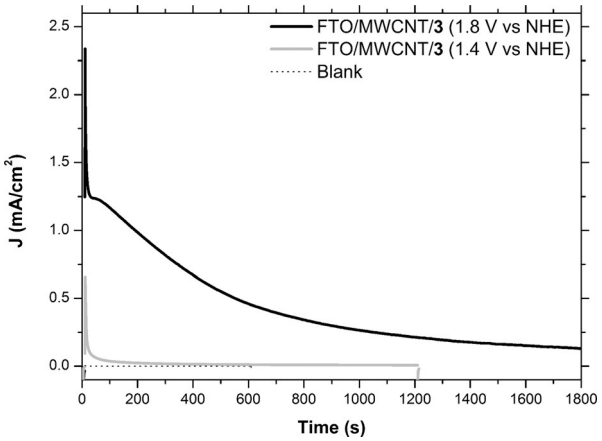

Figure 12. Prolonged activity of FTO/MWCNT/**3** at 1.4 and 1.8 V vs NHE in 0.1 M phosphate buffer solution at pH 2.0.

Conclusion

A water oxidation catalyst (NHC IrCp*Cl_2) has been successfully attached to a cationic pyrene anchor. This system acts as an efficient dispersing agent of multiwalled carbon nanotubes in aqueous solutions by the formation of MWCNT/Pyr^+ assemblies under neutral and acidic conditions. The MWCNT/Pyr^+ assembly was deposited onto FTO surfaces and evaluated as a working electrode for the electrocatalytic oxidation of H_2O. When the electrode was loaded with nanotubes that contain precursor **3**, initially high current densities were observed at pH 2.0, which are ascribed to water oxidation. Although the high current density is very promising, the degradation of the FTO/MWCNT/Pyr^+ anode by oxidation of the pyrene anchoring group was also observed at potentials above 1.4 V vs NHE, limiting the use of the current system. For the future design of related systems the anchoring group should be more stable under these oxidative conditions.

Acknowledgements

This study was carried out within the research programme of Bio-Solar Cells, co-financed by the Dutch Ministry of Economic Affairs.

Keywords: carbon nanotubes · catalysis · catalyst immobilization · electrodes · water splitting

[1] S. X. Guo, Y. P. Liu, C. Y. Lee, M. Bond, J. Zhang, Y. V. Geletiib, C. L. Hill, *Energy Environ. Sci.* **2013**, *6*, 2654 – 2663.
[2] Z. Chen, J. J. Concepcion, J. F. Hull, P. G. Hoertz, T. J. Meyer, *Dalton Trans.* **2010**, *39*, 6950 – 6952.
[3] L. Francàs, X. Sala, J. Benet-Buchholz, L. Escriche, A. Llobet, *ChemSusChem* **2009**, *2*, 321 – 329.
[4] F. Liu, T. Cardolaccia, B. J. Hornstein, J. R. Schoonover, T. J. Meyer, *J. Am. Chem. Soc.* **2007**, *129*, 2446 – 2447.
[5] D. M. Ryan, M. K. Coggins, J. J. Concepcion, D. L. Ashford, Z. Fang, L. Alibabaei, D. Ma, T. J. Meyer, M. L. Waters, *Inorg. Chem.* **2014**, *53*, 8120 – 8128.
[6] J. J. Concepcion, J. W. Jurss, P. G. Hoertz, T. J. Meyer, *Angew. Chem. Int. Ed.* **2009**, *48*, 9473 – 9476; *Angew. Chem.* **2009**, *121*, 9637 – 9640.
[7] T. Wada, K. Tsuge, K. Tanaka, *Angew. Chem. Int. Ed.* **2000**, *39*, 1479 – 1482; *Angew. Chem.* **2000**, *112*, 1539 – 1542.
[8] K. C. Pillai, A. S. Kumar, J. Zen, *J. Mol. Catal. A* **2000**, *160*, 277 – 285.
[9] J. Mola, E. Mas-Marza, X. Sala, I. Romero, M. Rodríguez, C. Viñas, T. Parella, A. Llobet, *Angew. Chem. Int. Ed.* **2008**, *47*, 5830 – 5832; *Angew. Chem.* **2008**, *120*, 5914 – 5916.
[10] H. Shiroishi, H. Sayama, T. Moroi, M. Kaneko, *J. Electroanal. Chem.* **2001**, *502*, 132 – 137.
[11] M. Yagi, E. Takano, M. Kaneko, *Electrochim. Acta* **1999**, *44*, 2493 – 2497.
[12] Z. Chen, J. J. Concepcion, J. W. Jurss, T. J. Meyer, *J. Am. Chem. Soc.* **2009**, *131*, 15580 – 1.
[13] M. Zhang, M.-T. Zhang, C. Hou, Z.-F. Ke, T.-B. Lu, *Angew. Chem. Int. Ed.* **2014**, *53*, 13042 – 13048; *Angew. Chem.* **2014**, *126*, 13258 – 13264.
[14] M. K. Coggins, M.-T. Zhang, A. K. Vannucci, C. J. Dares, T. J. Meyer, *J. Am. Chem. Soc.* **2014**, *136*, 5531 – 4.
[15] M. K. Coggins, M.-T. Zhang, Z. Chen, N. Song, T. J. Meyer, *Angew. Chem. Int. Ed.* **2014**, *53*, 12226 – 12230; *Angew. Chem.* **2014**, *126*, 12422 – 12426.
[16] L.-Z. Fu, T. Fang, L.-L. Zhou, S.-Z. Zhan, *RSC Adv.* **2014**, *4*, 53674 – 53680.
[17] X.-J. Su, M. Gao, L. Jiao, R.-Z. Liao, P. E. M. Siegbahn, J.-P. Cheng, M.-T. Zhang, *Angew. Chem. Int. Ed.* **2015**, *54*, 4909 – 4914.
[18] L.-L. Zhou, T. Fang, J.-P. Cao, Z.-H. Zhu, X.-T. Su, S.-Z. Zhan, *J. Power Sources* **2015**, *273*, 298 – 304.
[19] M. Felhendler, G. Ginzburg, D. Meyerstein, *J. Electroanal. Chem. Interfacial Electrochem.* **1980**, *112*, 295 – 309.
[20] T. Fang, L.-Z. Fu, L.-L. Zhou, S.-Z. Zhan, *Electrochim. Acta* **2015**, *161*, 388 – 394.
[21] X. Zhou, T. Zhang, C. W. Abney, Z. Li, W. Lin, *ACS Appl. Mater. Interfaces* **2014**, *6*, 18475 – 18479.
[22] D. L. Gerlach, S. Bhagan, A. A. Cruce, D. B. Burks, I. Nieto, H. T. Truong, S. P. Kelley, C. J. Herbst-Gervasoni, K. L. Jernigan, M. K. Bowman, S. Pan, M. Zeller, E. T. Papish, *Inorg. Chem.* **2014**, *53*, 12689 – 98.
[23] M.-T. Zhang, Z. Chen, P. Kang, T. J. Meyer, *J. Am. Chem. Soc.* **2013**, *135*, 2048 – 51.
[24] S. M. Barnett, K. I. Goldberg, J. M. Mayer, *Nat. Chem.* **2012**, *4*, 498 – 502.
[25] A. Han, H. Jia, H. Ma, S. Ye, H. Wu, H. Lei, Y. Han, R. Cao, P. Du, *Phys. Chem. Chem. Phys.* **2014**, *16*, 11209 – 17.
[26] H. Lei, A. Han, F. Li, M. Zhang, Y. Han, P. Du, W. Lai, R. Cao, *Phys. Chem. Chem. Phys.* **2014**, *16*, 1883 – 93.
[27] I. Siewert, J. Galezowska, *Chemistry* **2014**, *956*, 2780 – 2784.
[28] D. K. Dogutan, R. McGuire, D. G. Nocera, *J. Am. Chem. Soc.* **2011**, *133*, 9178 – 80.
[29] D. J. Wasylenko, R. D. Palmer, E. Schott, C. P. Berlinguette, *Chem. Commun.* **2012**, *48*, 2107 – 9.
[30] F. Yu, F. Li, B. Zhang, H. Li, L. Sun, *ACS Catal.* **2015**, *5*, 627 – 630.
[31] X. Liu, S. Cui, Z. Sun, P. Du, *Electrochim. Acta* **2015**, *160*, 202 – 208.
[32] D. Ressnig, M. Shalom, J. Patscheider, R. Moré, F. Evangelisti, M. Antonietti, G. R. Patzke, *J. Mater. Chem. A* **2015**, *3*, 5072 – 5082.
[33] B. H. R. Suryanto, X. Lu, H. M. Chan, C. Zhao, *RSC Adv.* **2013**, *3*, 20936.
[34] R. D. L. Smith, M. S. Pre, R. D. Fagan, S. Trudel, **2013**, *135*, 11580 – 11586.
[35] J. J. Stracke, R. G. Finke, *J. Am. Chem. Soc.* **2011**, *133*, 14872 – 14875.
[36] C. A. Kent, J. J. Concepcion, C. J. Dares, D. A. Torelli, A. J. Rieth, A. S. Miller, P. G. Hoertz, T. J. Meyer, *J. Am. Chem. Soc.* **2013**, *135*, 8432 – 8435.
[37] A. Han, H. Wu, Z. Sun, H. Jia, Z. Yan, X. Liu, P. Du, *ACS Appl. Mater. Interfaces* **2014**, *6*, 10929 – 10934.
[38] M. W. Kanan, D. G. Nocera, *Science* **2008**, *321*, 1072 – 1075.
[39] Y. Surendranath, M. W. Kanan, D. G. Nocera, *J. Am. Chem. Soc.* **2010**, *132*, 16501 – 16509.
[40] D. G. Nocera, *Acc. Chem. Res.* **2012**, *45*, 767 – 776.
[41] M. Dinca, Y. Surendranath, D. G. Nocera, *Proc. Natl. Acad. Sci. USA* **2010**, *107*, 10337 – 41.
[42] K. S. Joya, N. K. Subbaiyan, F. D'Souza, H. J. M. de Groot, *Angew. Chem. Int. Ed.* **2012**, *51*, 9601 – 9605; *Angew. Chem.* **2012**, *124*, 9739 – 9743.
[43] O. Diaz-Morales, T. J. P. Hersbach, D. G. H. Hetterscheid, J. N. H. Reek, M. T. M. Koper, *J. Am. Chem. Soc.* **2014**, *136*, 10432 – 10439.
[44] S. W. Sheehan, J. M. Thomsen, U. Hintermair, R. H. Crabtree, G. W. Brudvig, C. A. Schmuttenmaer, *Nat. Commun.* **2015**, *6*, 6469.
[45] N. D. Schley, J. D. Blakemore, N. K. Subbaiyan, C. D. Incarvito, F. Dsouza, R. H. Crabtree, G. W. Brudvig, *J. Am. Chem. Soc.* **2011**, *133*, 10473 – 10481.
[46] M. Yagi, E. Tomita, T. Kuwabara, *J. Electroanal. Chem.* **2005**, *579*, 83 – 88.
[47] M. N. Kushner-Lenhoff, J. D. Blakemore, N. D. Schley, R. H. Crabtree, G. W. Brudvig, *Dalton Trans.* **2013**, *42*, 3617 – 3622.
[48] M. Vukovic, *J. Appl. Electrochem.* **1987**, *17*, 737 – 745.
[49] A. Harriman, I. J. Pickering, J. M. Thomas, P. a. Christensen, *J. Chem. Soc. Faraday Trans. 1* **1988**, *84*, 2795.
[50] N. Nakashima, Y. Tanaka, Y. Tomonari, H. Murakami, H. Kataura, T. Sakaue, K. Yoshikawa, *J. Phys. Chem. B* **2005**, *109*, 13076 – 13082.
[51] Y. Tomonari, H. Murakami, N. Nakashima, *Chem. Eur. J.* **2006**, *12*, 4027 – 4034.
[52] N. Nakashima, Y. Tomonari, H. Murakami, *Chem. Lett.* **2002**, 638 – 638.
[53] M. O. F. Khan, S. E. Austin, C. Chan, H. Yin, D. Marks, S. N. Vaghjiani, H. Kendrick, V. Yardley, S. L. Croft, K. T. Douglas, *J. Med. Chem.* **2000**, *43*, 3148 – 3156.
[54] E. C. Buruiana, T. Buruiana, M. Zamfir, V. Pohoata, D. Donescu, *Des. Monomers Polym.* **2007**, *10*, 347 – 360.
[55] F. Ito, T. Kakiuchi, T. Sakano, T. Nagamura, *Phys. Chem. Chem. Phys.* **2010**, *12*, 10923 – 7.
[56] F. Ito, T. Sagawa, H. Koshiyama, *Res. Chem. Intermed.* **2015**, *41*, 6897 – 6906.
[57] S. Detriche, S. Devillers, J. F. Seffer, J. B. Nagy, Z. Mekhalif, J. Delhalle, *Carbon* **2011**, *49*, 2935 – 2943.
[58] J. Liu, F. Appaix, O. Bibari, G. Marchand, A.-L. Benabid, F. Sauter-Starace, M. De Waard, *Nanotechnology* **2011**, *22*, 195101.
[59] A. Viinikanoja, J. Kauppila, P. Damlin, E. Makila, J. Leiro, T. Aaritalo, J. Lukkari, *Carbon* **2014**, *68*, 195 – 209.
[60] C.-L. Chung, C. Gautier, S. Campidelli, A. Filoramo, *Chem. Commun.* **2010**, *46*, 6539 – 6541.
[61] G. Pagona, A. S. D. Sandanayaka, A. Maigné, J. Fan, G. C. Papavassiliou, I. D. Petsalakis, B. R. Steele, M. Yudasaka, S. Iijima, N. Tagmatarchis, O. Ito, *Chemistry* **2007**, *13*, 7600 – 7.
[62] D. M. Guldi, G. M. A. Rahman, N. Jux, D. Balbinot, N. Tagmatarchis, M. Prato, *Chem. Commun.* **2005**, 2038 – 40.
[63] D. M. Guldi, G. M. A. Rahman, N. Jux, N. Tagmatarchis, M. Prato, *Angew. Chem. Int. Ed.* **2004**, *43*, 5526 – 5530; *Angew. Chem.* **2004**, *116*, 5642 – 5646.
[64] G. Pagona, J. Fan, A. Maignè, M. Yudasaka, S. Iijima, N. Tagmatarchis, *Diamond Relat. Mater.* **2007**, *16*, 1150 – 1153.
[65] G. Katsukis, J. Malig, C. Schulz-Drost, S. Leubner, N. Jux, D. M. Guldi, *ACS Nano* **2012**, *6*, 1915 – 1924.
[66] J. Malig, C. Romero-Nieto, N. Jux, D. M. Guldi, *Adv. Mater.* **2012**, *24*, 800 – 805.
[67] C. Ehli, G. M. A. Rahman, N. Jux, D. Balbinot, D. M. Guldi, F. Paolucci, M. Marcaccio, D. Paolucci, M. Melle-Franco, F. Zerbetto, S. Campidelli, M. Prato, *J. Am. Chem. Soc.* **2006**, *128*, 11222 – 31.
[68] N. Tagmatarchis, M. Prato, D. M. Guldi, *Phys. E* **2005**, *29*, 546 – 550.

[69] D. M. Guldi, G. M. A. Rahman, M. Prato, N. Jux, S. Qin, W. Ford, *Angew. Chem. Int. Ed.* **2005**, *44*, 2015 – 2018; *Angew. Chem.* **2005**, *117*, 2051 – 2054.
[70] G. M. A. Rahman, D. M. Guldi, R. Cagnoli, A. Mucci, L. Schenetti, L. Vaccari, M. Prato, *J. Am. Chem. Soc.* **2005**, *127*, 10051 – 10057.
[71] V. Sgobba, A. Troeger, R. Cagnoli, A. Mateo-Alonso, M. Prato, F. Parenti, A. Mucci, L. Schenetti, D. M. Guldi, *J. Mater. Chem.* **2009**, *19*, 4319.
[72] F. M. Toma, A. Sartorel, M. Iurlo, M. Carraro, S. Rapino, L. Hoober-Burkhardt, T. Da Ros, M. Marcaccio, G. Scorrano, F. Paolucci, M. Bonchio, M. Prato, *ChemSusChem* **2011**, *4*, 1447 – 1451.
[73] F. M. Toma, A. Sartorel, M. Iurlo, M. Carraro, P. Parisse, C. Maccato, S. Rapino, B. R. Gonzalez, H. Amenitsch, T. Da Ros, L. Casalis, A. Goldoni, M. Marcaccio, G. Scorrano, G. Scoles, F. Paolucci, M. Prato, M. Bonchio, *Nat. Chem.* **2010**, *2*, 826 – 31.
[74] F. Li, B. Zhang, X. Li, Y. Jiang, L. Chen, Y. Li, L. Sun, *Angew. Chem. Int. Ed.* **2011**, *50*, 12276 – 12279; *Angew. Chem.* **2011**, *123*, 12484 – 12487.
[75] F. Li, L. Li, L. Tong, Q. Daniel, M. Göthelid, L. Sun, *Chem. Commun.* **2014**, *50*, 13948 – 13951.
[76] Y.-X. Zhang, X. Guo, X. Zhai, Y.-M. Yan, K.-N. Sun, *J. Mater. Chem. A* **2015**, *3*, 1761 – 1768.
[77] D. Ye, T. Wu, H. Cao, Y. Wang, B. Liu, S. Zhang, J. Kong, *RSC Adv.* **2015**, *5*, 26710 – 26715.
[78] X. Yu, P. Xu, T. Hua, A. Han, X. Liu, H. Wu, P. Du, *Int. J. Hydrogen Energy* **2014**, *39*, 10467 – 10475.
[79] X. Lu, C. Zhao, *J. Mater. Chem. A* **2013**, *1*, 12053.
[80] X. Zhai, W. Yang, M. Li, G. Lv, J. Liu, X. Zhang, *Carbon* **2013**, *65*, 277 – 286.
[81] K. Mette, A. Bergmann, J.-P. Tessonnier, M. Hävecker, L. Yao, T. Ressler, R. Schlögl, P. Strasser, M. Behrens, *ChemCatChem* **2012**, *4*, 851 – 862.
[82] X. Lu, W.-L. Yim, B. H. R. Suryanto, C. Zhao, *J. Am. Chem. Soc.* **2015**, *137*, 2901 – 2907.
[83] Y. Cheng, C. W. Xu, L. C. Jia, J. D. Gale, L. L. Zhang, C. Liu, P. K. Shen, S. P. Jiang, *Appl. Catal. B* **2015**, *163*, 96 – 104.
[84] A. Venturini, A. Barbieri, J. N. H. Reek, D. G. H. Hetterscheid, *Chemistry* **2014**, *20*, 5358 – 68.
[85] D. G. H. Hetterscheid, J. N. H. Reek, *Chem. Commun.* **2011**, *47*, 2712.
[86] D. G. H. Hetterscheid, J. N. H. Reek, *Eur. J. Inorg. Chem.* **2014**, 742 – 749.
[87] J. M. Koelewijn, M. Lutz, W. I. Dzik, R. J. Detz, J. N. H. Reek, *ACS Catal.* **2016**, *6*, 3418 – 3427.
[88] X.-Q. Xiao, G.-X. Jin, *J. Organomet. Chem.* **2008**, *693*, 3363 – 3368.
[89] P. Kang, S. Zhang, T. J. Meyer, M. Brookhart, *Angew. Chem. Int. Ed.* **2014**, *53*, 8709 – 8713; *Angew. Chem.* **2014**, *126*, 8853 – 8857.
[90] P. D. Tran, A. Le Goff, J. Heidkamp, B. Jousselme, N. Guillet, S. Palacin, H. Dau, M. Fontecave, V. Artero, *Angew. Chem. Int. Ed.* **2011**, *50*, 1371 – 1374; *Angew. Chem.* **2011**, *123*, 1407 – 1410.
[91] J. D. Blakemore, A. Gupta, J. J. Warren, B. S. Brunschwig, H. B. Gray, *J. Am. Chem. Soc.* **2013**, *135*, 18288 – 18291.
[92] CCDC 1478159 and 1478160 contain the supplementary crystallographic data for this paper. These data can be obtained free of charge from The Cambridge Crystallographic Data Centre.

Manuscript received: May 4, 2016
Accepted Article published: June 7, 2016
Final Article published: July 7, 2016